Available online at www.sciencedirect.com
SCIENCE DIRECT®
Journal of Power Sources 115 (2003) 119–124
JOURNAL OF POWER SOURCES
www.elsevier.com/locate/jpowsour

Electrochemical insertion of lithium and sodium into $(MoO_2)_2P_2O_7$

Yasushi Uebou*, Shigeto Okada, Jun-ichi Yamaki

Institute of Advanced Material Study, Kyushu University, Kasuga-Koen, Kasuga, Fukuoka 816-8580, Japan

Received 5 August 2002; received in revised form 18 November 2002; accepted 28 November 2002

Abstract

Insertion of lithium and sodium into phosphate $(MoO_2)_2P_2O_7$ was investigated electrochemically to determine the usefulness as a possible cathode for ion-transfer secondary batteries. Specific charges of up to 250 mA h g^{-1} were obtained for A/$(MoO_2)_2P_2O_7$ (A: Li, Na) cells with liquid organic electrolytes in the first reduction half-cycle at room temperature. Intercalation processes under constant current densities of 0.2 mA cm^{-2} were reversible within the range of composition $0.85 < x < 4.0$ for lithium and $0.5 < x < 3.1$ for sodium in $A_x(MoO_2)_2P_2O_7$ (A: Li, Na), respectively. Structural changes induced by lithium or sodium intercalation were followed by ex situ X-ray diffraction measurements, and the phase change from the crystal to the amorphous was observed in both cases.

Keywords: Phosphate; Lithium; Sodium; Insertion

1. Introduction

Lithium transition metal dioxides with the general formula $LiMO_2$ (M: V, Cr, Fe, Co, Ni) are seen to have the structure of α-$NaFeO_2$, which can be regarded as a distorted rock salt-type structure. $LiCoO_2$ and $LiNiO_2$ used as cathodes for secondary lithium ion batteries have assumed an industrial importance [1–6]. At the same time, a number of materials have been synthesized and evaluated for use as the cathode-active material in lithium secondary batteries. Examples of the such materials include: spinel-type, $Li_2MMn_3O_8$ and $LiM'MnO_4$ (M: Cr [7,8], Fe [9], Co [10], Ni [11,12], Cu [13,14]; M′: Cr [7,8], Co [15]); inverse spinel-type, $LiMVO_4$ (M: Ni, Co) [16]; layered-type, $LiMnO_2$ [17–19], and so on.

The vast majority of studies have been directed toward the promising lithium system, but recent results obtained on $NaMO_2$ (M: Co, Ni) [20] and α-$NaFeO_2$–MoO_3 [21] prove that sodium cells can function with liquid organic electrolytes at room temperature. However, improvement in energy density and rate capability is required before sodium/liquid organic electrolyte batteries can be considered for practical use. Because of the lower capacity density and less negative voltage [versus standard hydrogen electrode (SHE)] compared to lithium, energy densities are expected to be lower for cells utilizing sodium. Additionally, host materials commonly used as cathodes tend to intercalate sodium to a lesser extent than lithium due to the larger ionic radius, further reducing energy densities. Still, the comparatively lower cost of sodium [22] makes development of sodium/liquid organic electrolyte systems a compelling goal (Table 1).

Clearly, the challenge is to find a cathode material that can intercalate sodium to a large extent and thus allow a high theoretical energy density in sodium batteries. Recently, polyanionic compounds that exhibit framework structures built up from both (MO_n) polyhedra and $(XO_4)^{m-}$ tetrahedra polyanions (M: transition metal; X: S [23,24], P [24]) instead of only (MO_n) polyhedra in transition oxides, have attracted considerable attention. The main reason is that lithium and sodium ions can both be inserted into a series of compounds having a general formula of $A_nM_2(XO_4)_3$ (A: Li and Na; M: Ti [25], Fe [26]; X: P [25], S [26]), because they have a large lithium or sodium site based on the 3D framework. In addition, their operating voltage can be tuned by the crystal structure as well as by the choice of the counter-cation, X. It has been shown in previous works on $Li_xFe_2(XO_4)_3$ (X: Mo, W, S, P) [27,28] compounds that the Fe^{3+}/Fe^{2+} redox couple lies at 3.0, 3.0, 3.6, and 2.8 V versus Li/Li^+, and from the viewpoint of crystal structure, the Fe^{3+}/Fe^{2+} redox couple versus Li/Li^+ in four iron phosphates, NASICON-type $Li_3Fe_2(PO_4)_3$ [27], the pyrophosphates $LiFeP_2O_7$ [27] and $Fe_4(P_2O_7)_3$ [27], and olivine-type $LiFePO_4$ [27], lies at 2.8, 2.9, 3.1, and 3.5 V, respectively. Although some of these phosphates, such as NASICON-type $NaTi_2(PO_4)_3$ and $Fe_2(SO_4)_3$, are interesting as candidates for

* Corresponding author. Tel.: +81-92-583-7792; fax: +81-92-583-7790.
E-mail address: uebou@asem.kyushu-u.ac.jp (Y. Uebou).

0378-7753/03/$ – see front matter
doi:10.1016/S0378-7753(02)00648-1

Table 1
Characteristics of anode materials

Characteristic	Sodium	Lithium
Cost equivalent of dollars for bulk metal	0.075	0.50
Capacity density (A h g^{-1})	1.06	3.86
V vs. SHE	−2.71	−3.05
Ionic radius (Å)	0.98	0.68

the high-voltage cathode material for sodium batteries, the gravimetric energy densities of those materials with liquid organic electrolytes at room temperature remain at 280 and 250 W h kg^{-1}, respectively.

In the present study, we synthesized $(MoO_2)_2P_2O_7$ phosphate, and investigated the detailed crystal structure by the Rietveld method. Moreover, we paid attention not only to its open structure and flexibility but also to the possibility of reducing Mo^{6+} by eventual intercalation of alkali metals, and its potential for use as the new cathode material for lithium and sodium batteries was discussed.

2. Experimental

The $(MoO_2)_2P_2O_7$ powder sample was prepared by conventional solid reaction methods. Starting materials were α-$NaFeO_2$–MoO_3 (99.0% Wako) and P_2O_5 (98.0% Wako). These reagents were mixed in stoichiometric ratio then the mixture was heated at 500–700 °C for 6–24 h in air. The obtained powder sample was identified by powder X-ray diffractometer (Rigaku RINT2100HLR/PC) with Cu Kα–$NaFeO_2$ radiation. The structures were determined by Rietveld analysis using the computer program RIETAN97-β [29]. Mo K-edge XAFS spectra were measured by transmission mode using a laboratory-type XAFS facility, R-XAS Looper (Rigaku Corporation). An X-ray generator with a Mo rotating anode and a LaB_6 cathode was operated at a voltage of 36 kV and a current of 30 mA. The incident X-ray beam was monochromatized using Ge (840) crystal. The samples for the electrochemical measurement were prepared by mixing crystalline $(MoO_2)_2P_2O_7$, acetylene black as the conductive agent and PTFE Teflon binder (70, 25, and 5 wt.%, respectively) in an agate mortar, and were made in sheet form (1 mm thick). The sheet was then cut into a disk (15 mm diameter). Cells were fabricated by coupling this disk with lithium or sodium foil with the same area as counter-electrode using microporous polypropylene film (Celgard 3501) as the separator. $LiPF_6$ solution (1 M) in ethylene carbonate (EC)/1,2 dimethoxycarbonate (DMC) (volume ratio = 1:1) for lithium cells, and 1 M $NaClO_4$ solution in propylene carbonate (PC) for sodium cells were used as the electrolytes, respectively. The electrochemical measurements were carried out galvanostatically at various current densities at room temperature. In the quasi-open circuit voltage measurements, a current density of 0.2 mA cm^{-2} was used; the current density was applied for 75 min, and the system was relaxed for another 75 min before the data was read. To avoid humidity, the cathode pellets lithiated at various depths were covered with polyethylene film. They were then subjected to ex situ XRD measurements in order to observe the crystal structure change on the first cycle. Correction of the line positions was carried out using silicon powder (NIST 640c) as the internal standard.

3. Results and discussion

3.1. Synthesis and structure

Indexing of the powder X-ray pattern of $(MoO_2)_2P_2O_7$ synthesized at 700 °C for 24 h revealed that the sample had a

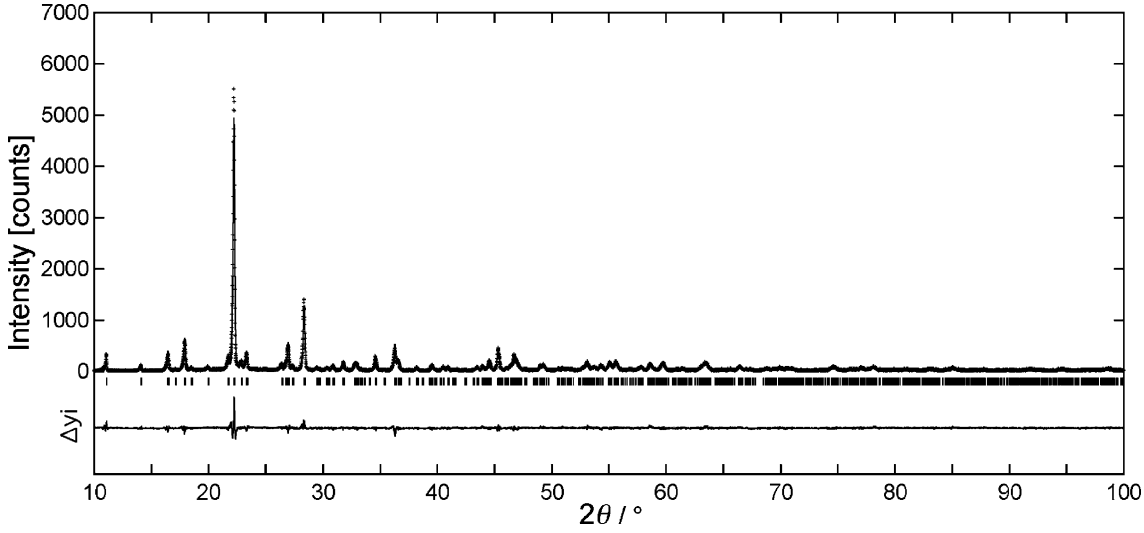

Fig. 1. Observed, calculated, and difference plots for X-ray diffraction patterns of $(MoO_2)_2P_2O_7$. The solid line is calculated intensity, dots overlying them are observed intensity, and Δy_i is the difference between observed and calculated intensity.

single phase with an orthorhombic lattice. However, the relative intensities of the X-ray patterns were different from that in the ICDD file (no. 15-0610). Thus, we attempted to refine the structure of $(MoO_2)_2P_2O_7$ by the Rietveld method on the space group *Pnma* (no. 62), using a structural model reported by Kierkegaard [30]. At first, we assumed no correction for the preferred orientation, but a difference between the observed and the calculated pattern was observed in the (1 0 1) direction. Therefore, correction for the (1 0 1) direction was made. The site occupation parameter of g and the overall thermal parameters B for all sites were constrained to be the same value. We assume that the cause of the difference between the observed data and the ICDD file was mainly attributable to the preferred orientation. The fitting results are illustrated in Fig. 1. The schematic diagram of the crystal structure obtained by Rietveld refinement is shown in Fig. 2. The possible cavities for lithium or sodium insertion are indicated as (∗). The lattice parameters were indexed by an orthorhombic cell with dimensions $a = 12.580(4)$, $b = 6.302(18)$, and $c = 10.366(2)$ Å. In comparison with reported values for $(MoO_2)_2P_2O_7$ [30], $a = 12.58$, $b = 6.338$, and $c = 10.38$ Å, slight decreases of b and c axis parameters were observed. Table 2 lists the final R factors, structural parameters and their estimated standard deviations. Fig. 3 shows the XANES spectra corresponding to the Mo K-edge for $(MoO_2)_2P_2O_7$ with α-$NaFeO_2$–MoO_3 as the standard Mo(VI) compound. No significant difference was observed among them, which indicates that the valence states of Mo are also 6+ in $(MoO_2)_2P_2O_7$.

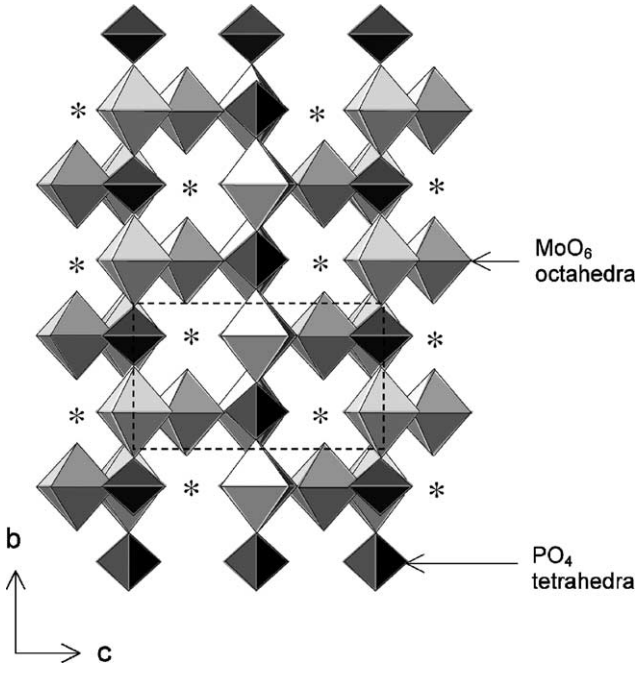

Fig. 2. The structure of $(MoO_2)_2P_2O_7$. The possible cavities for lithium or sodium insertion are indicated as (∗).

Table 2
X-ray Rietveld refinement results for monoclinic $(MoO_2)_2P_2O_7$[a]

Atom	Site	x	y	z	B (Å^2)
Mo(1)	4*c*	0.996(2)	0.25	0.224(2)	0.4
Mo(2)	4*c*	0.252(2)	0.25	0.014(2)	Mo(1)
P(1)	4*c*	0.659(7)	0.25	0.994(8)	Mo(1)
P(2)	4*c*	0.971(7)	0.25	0.694(7)	Mo(1)
O(1)	8*d*	0.271(9)	0.572(19)	0.019(10)	Mo(1)
O(2)	8*d*	0.016(12)	0.566(18)	0.222(9)	Mo(1)
O(3)	4*c*	0.910(13)	0.25	0.580(15)	Mo(1)
O(4)	4*c*	0.580(13)	0.25	0.102(16)	Mo(1)
O(5)	4*c*	0.099(14)	0.25	0.631(16)	Mo(1)
O(6)	4*c*	0.165(12)	0.25	0.147(15)	Mo(1)
O(7)	4*c*	0.377(12)	0.25	0.188(15)	Mo(1)
O(8)	4*c*	0.179(13)	0.25	0.884(15)	Mo(1)
O(9)	4*c*	0.459(13)	0.25	0.425(16)	Mo(1)

[a] Space group: *Pnma*; $a = 12.580(4)$, $b = 6.302(18)$, and $c = 10.366(2)$ Å; $R_{wp} = 16.77\%$; $R_e = 12.17\%$; $R_I = 6.07\%$; and $S = 1.378(3)$.

3.2. Lithium and sodium insertion behavior

Fig. 4 shows the quasi-open circuit voltage curves for A/$(MoO_2)_2P_2O_7$ (A: Li, Na) and Li/α-$NaFeO_2$–MoO_3 cells as a function of lithium or sodium content, x (upper) and capacity (lower), with a current density of 0.2 mA cm^{-2} at room temperature. $(MoO_2)_2P_2O_7$ was able to accommodate the lithium and sodium ion, and the quasi-open circuit voltage at early region ($0 < x < 2.5$) for Li/$(MoO_2)_2P_2O_7$ cell was higher than that of the transition metal oxide α-$NaFeO_2$–MoO_3. Similar cell voltage enhancement via the inductive effect of hetero atoms was observed in V and Ti pyrophosphate cathodes as well as in NASICON and olivine-type cathodes. For example, the M^{4+}/M^{3+} (M: V, Ti) redox potentials versus Li/Li^+ in the pyrophosphates $LiVP_2O_7$ [31,32] and TiP_2O_7 [32] lies at 4.1 V and 2.6 V, respectively, and were higher than those of the transition metal oxides,

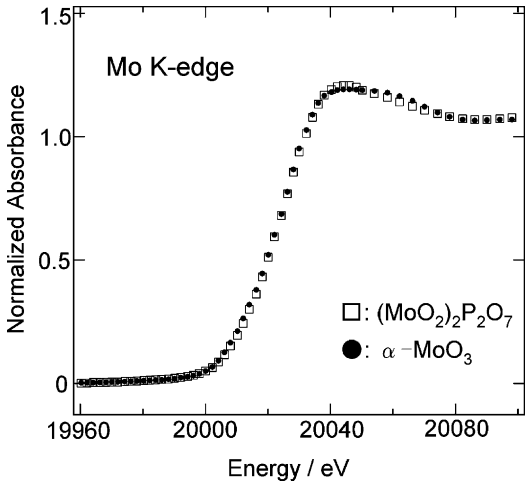

Fig. 3. Mo K-edge XANES spectra of $(MoO_2)_2P_2O_7$ and α-$NaFeO_2$–MoO_3.

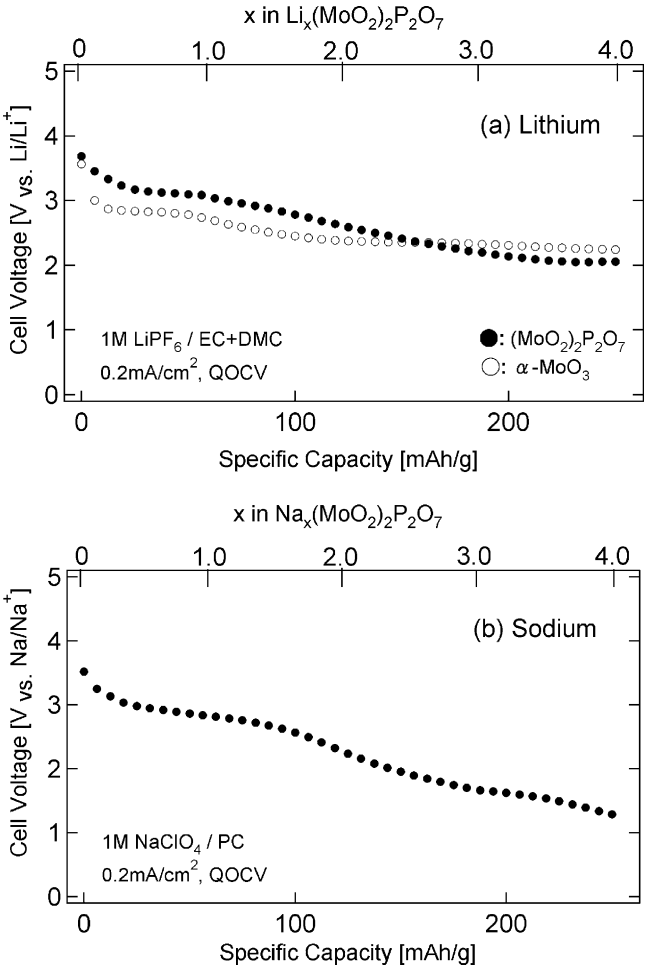

Fig. 4. Discharging curves of A (A: (a) Li, (b) Na)/electrolyte/$(MoO_2)_2P_2O_7$ and α-$NaFeO_2$–MoO_3 cells with galvanostatic intermittently run under the following experimental condition: 0.2 mA cm^{-2} current density was applied for 75 min and the system was allowed to relax for 75 min at room temperature.

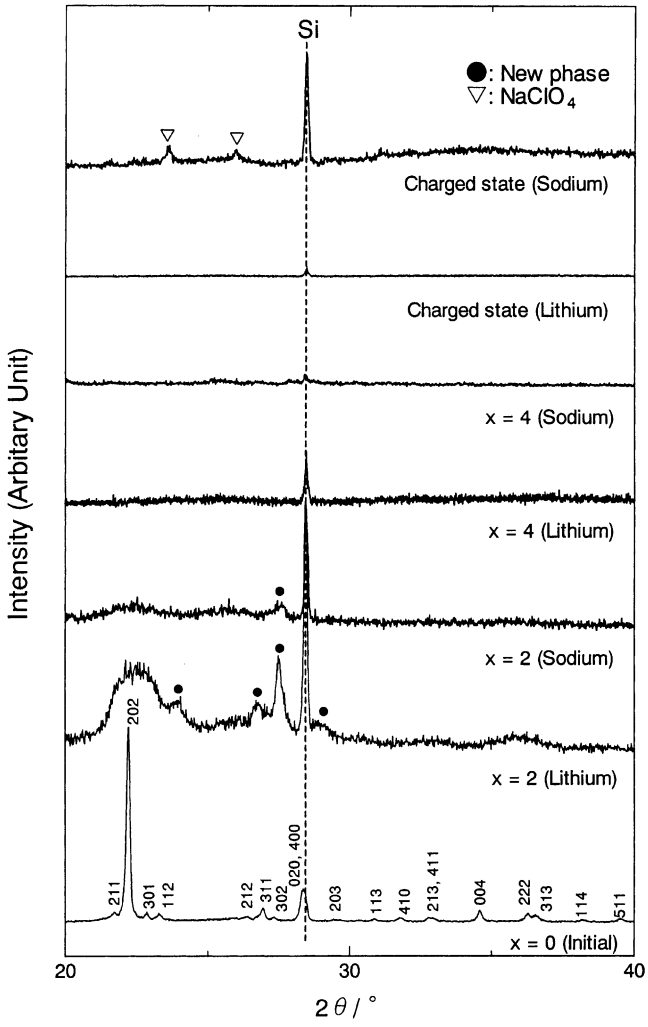

Fig. 5. XRD patterns of the electrode at various discharge and charged states as a function of lithium or sodium content; x for $A_x(MoO_2)_2P_2O_7$ (A: Li, Na).

VO_2 and rutile TiO_2, which lies at 2.5 [33] and 1.4 V, respectively [34]. The similar quasi-open circuit voltage curve of $Li/(MoO_2)_2P_2O_7$ and $Na/(MoO_2)_2P_2O_7$ cells, shown in Fig. 4, suggests that lithium and sodium ions insert into the same site in the $(MoO_2)_2P_2O_7$ matrix. The discharge capacities of $(MoO_2)_2P_2O_7$ cathodes during the first cycle at room temperature were about 250 mA h g^{-1} at 2.0–3.7 V versus Li/Li^+, and at 1.2–3.5 V versus Na/Na^+, respectively. In terms of the discharge capacity for the first cycle, the $Li/(MoO_2)_2P_2O_7$ cell showed a fairly good performance, which was better than those of the pyrophosphates that contained Fe, V, and Ti. For example, the reported discharge capacity of both $Li/LiMP_2O_7$ (M: Fe, V) cells was 60 mA h g^{-1} [27,32], and that of the Li/TiP_2O_7 cell was 90 mA h g^{-1} [32]. Fig. 5 shows the X-ray diffraction patterns of the positive electrode at various discharge and charged states as a function of lithium or sodium content; x for $A_x(MoO_2)_2P_2O_7$ (A: Li, Na). The insertion of lithium or sodium decreased the initial peaks, and additional peaks appeared. The new phase could not be identified because of its weak intensity and high background, corresponding to amorphization. The irreversible change from the crystal to the amorphous phase induced by lithium insertion has been reported previously in molybdenum-based oxide $MnMoO_4$ [35]. Fig. 6 shows the discharge and charge curves for $A/(MoO_2)_2P_2O_7$ (A: Li, Na) cells with a current density of 0.2 mA cm^{-2} at room temperature in the voltage range of 1.9–4.2 V versus Li/Li^+, and of 1.2–3.8 V versus Na/Na^+, respectively. The lithium insertion into $(MoO_2)_2P_2O_7$ proceeded to $x = 4.0$ ($Li_{4.0}(MoO_2)_2P_2O_7$), which corresponded to 250 mA h g^{-1}. On the other hand, the sodium insertion into $(MoO_2)_2P_2O_7$ was limited to $x = 3.1$ ($Na_{3.1}(MoO_2)_2P_2O_7$), which corresponded to 190 mA h g^{-1}. Fig. 7 shows the discharge curves for $A/(MoO_2)_2P_2O_7$ (A: Li, Na) cells at various current densities at room temperature. The specific capacity of sodium insertion becomes

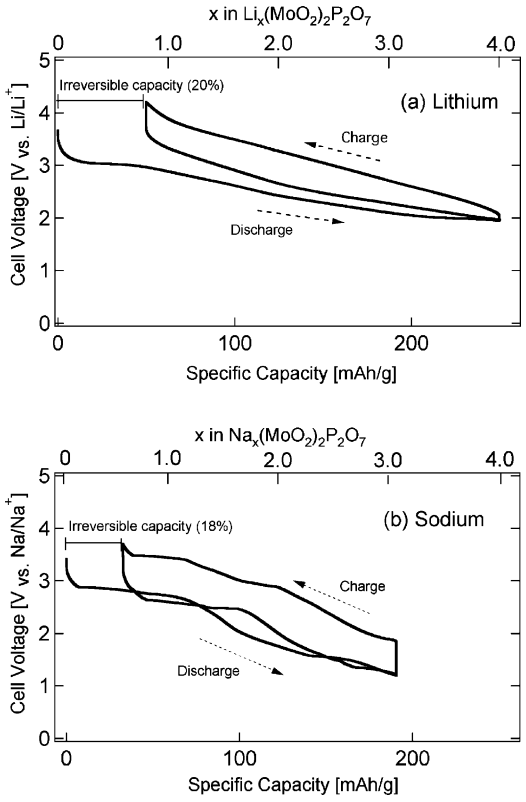

Fig. 6. Discharge and charge curves of A (A: (a) Li, (b) Na)/electrolyte/$(MoO_2)_2P_2O_7$ cells at a constant current density of 0.2 mA cm^{-2} at room temperature.

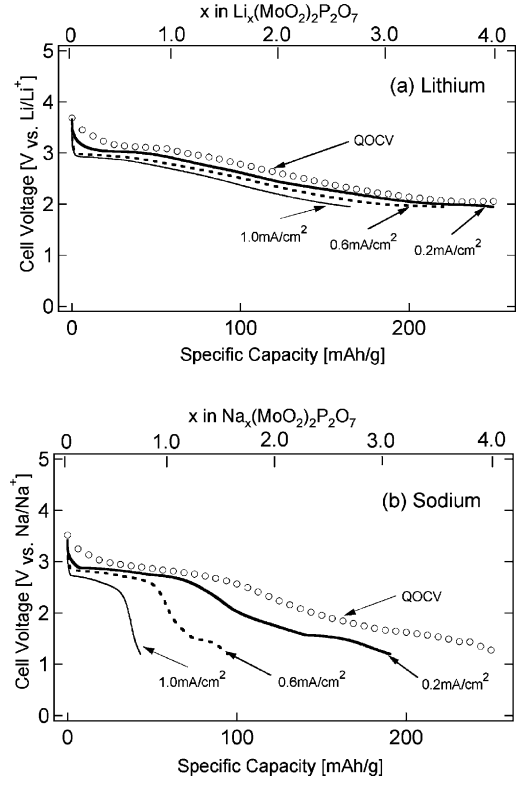

Fig. 7. Discharge curves of A (A: (a) Li, (b) Na)/electrolyte/$(MoO_2)_2P_2O_7$ cells at various current densities at room temperature.

small at the higher current density in comparison with that of lithium insertion. The poorer rate capability of Na/$(MoO_2)_2P_2O_7$ must be caused by the lower mobility of the comparatively larger sodium ion in the host lattice.

4. Conclusion

A study of the electrochemical lithium and sodium insertion in $(MoO_2)_2P_2O_7$ with liquid organic electrolytes at room temperature was carried out. It revealed that the quasi-open circuit voltage in $(MoO_2)_2P_2O_7$ (versus Li/Li^+) was higher than that of the transition metal oxide α-$NaFeO_2$–MoO_3. In terms of the discharge capacity for the first cycle and the observed capacity loss, the Li/$(MoO_2)_2P_2O_7$ cell showed better performance than those of other pyrophosphate cathodes with transition metals Fe, V, or Ti. However, the discharge voltage of the Na/$(MoO_2)_2P_2O_7$ cell was slightly lower than that of the Li/$(MoO_2)_2P_2O_7$ cell, $(MoO_2)_2P_2O_7$ was able to accommodate the sodium ion, which is larger than the lithium ion.

Acknowledgements

The authors are grateful to Hisashi Yashiro of Rigaku Corporation for his assistance in the XAFS measurement.

References

[1] M.S.G.R. Thomas, W.I.F. David, J.B. Goodenough, Mater. Res. Bull. 20 (1985) 1137.
[2] K. Mizushima, P.C. Jones, P.J. Wiseman, J.B. Goodenough, Mater. Res. Bull. 15 (1980) 783.
[3] C. Delmas, J.J. Braconnier, P. Hagenmuller, Mater. Res. Bull. 17 (1982) 117.
[4] A. Mendiboure, C. Delmas, P. Hagenmuller, Mater. Res. Bull. 19 (1984) 1383.
[5] K. Tozawa, in: Proceedings of Conference on Rechargeable Batteries, Tokyo, 1990.
[6] J. R. Dahn, U. von Sacken, R. Fong, in: Proceedings of the Abstracts of the Electrochem. Soc. Meeting, Abstract No. 42, Seattle, WA, 1990, p. 90.
[7] C. Sigala, D. Guyomard, A. Verbaere, Y. Piffard, M. Tournoux, Solid State Ionics 81 (1995) 167.
[8] C. Sigara, A. Verbaere, J.L. Mansot, D. Guyomard, Y. Piffard, M. Tournoux, J. Solid State Chem. 132 (1997) 372.
[9] H. Kawai, M. Nagata, M. Tabuchi, H. Tukamoto, A.R. West, Chem. Mater. 10 (1998) 3266.
[10] H. Kawai, M. Nagata, H. Tukamoto, A.R. West, J. Mater. Chem. 8 (1998) 837.
[11] Q. Zhong, A. Bonakdarpour, M. Zhang, Y. Gao, J.R. Dahn, J. Electrochem. Soc. 144 (1997) 205.
[12] K. Amine, H. Tukamoto, H. Yasuda, Y. Fujita, J. Power Sources 68 (1997) 604.
[13] Y. Ein-Eli, W.F. Howard, J. Electrochem. Soc. 144 (1997) L205.
[14] Y. Ein-Eli, W.F. Howard, S.H. Lu, S. Mukerjee, J. McBreen, J.T. Vaughey, M.M. Thackeray, J. Electrochem. Soc. 145 (1998) 1238.
[15] H. Kawai, M. Nagata, H. Tukamoto, A.R. West, J. Electrochem. Soc. 1 (1998) 212.

[16] G. Fey, W. Li, J.R. Dahn, J. Electrochem. Soc. 141 (1994) 2279.
[17] A.R. Armstrong, P.G. Bruce, Nature 381 (1996) 499.
[18] G. Vitins, K. West, J. Electrochem. Soc. 144 (1997) 2587.
[19] K. Ado, M. Tabuchi, H. Kobayashi, H. Kageyama, O. Nakamura, Y. Inaba, R. Kanno, M. Takagi, Y. Takeda, J. Electrochem. Soc. 144 (1997) L177.
[20] C. Delmas, J.J. Braconnier, A. Maazaz, P. Hagenmuller, Rev. Chim. Minerale 19 (1982) 343.
[21] M.E. Spahr, P. Novak, O. Haas, R. Nesper, J. Power Sources 54 (1995) 346.
[22] Chem. Marketing Rep. 243 (1993).
[23] A. Manthiram, J.B. Goodenough, J. Power Sources 26 (1989) 403.
[24] S. Okada, H. Arai, K. Asakura, Y. Sakurai, J. Yamaki, K.S. Nanjundaswamy, A.K. Padhi, C. Masquelier, J.B. Goodenough, Prog. Batteries Battery Mater. 16 (1997) 302.
[25] C. Delmas, A. Nadiri, Solid State Ionics 28 (1988) 419.
[26] S. Okada, H. Arai, J. Yamaki, DENKI KAGAKU 65 (1997) 802.
[27] A.K. Padhi, K.S. Nanjundaswamy, C. Masquelier, S. Okada, J.B. Goodenough, J. Electrochem. Soc. 144 (1997) 1609.
[28] A.K. Padhi, K.S. Nanjundaswamy, C. Masquelier, J.B. Goodenough, J. Electrochem. Soc. 144 (1997) 2581.
[29] F. Izumi, in: R.A. Young (Ed.), The Rietveld Method, Chapter 13, Oxford University Press, Oxford, 1993.
[30] P. Kierkegaard, Arkiv Kemi. 19 (1962) 51.
[31] M. Morcrette, C. Wurm, J. Gaubicher, C. Masquelier, Extended Abstract of Lithium Battery Discussion of Electrode Materials, Abstract No. 93, Arcachon, France, 27 May–1 June 2001.
[32] Y. Uebou, S. Okada, J. Yamaki, Solid State Ionics 148 (2002) 323.
[33] T. Ohzuku, K. Sawai, T. Hirai, Denchi Gijutu, Battery Technol. 3 (1991) 14.
[34] Z. Takehara, T. Ohzuku, S. Yoshizawa, Rep. Asahi Glass Found. Ind. Technol. 33 (1978) 75.
[35] S.S. Kim, S. Ogura, H. Ikuta, Y. Uchimoto, M. Wakihara, Solid State Ionics 146 (2002) 249.